

Boosting ferromagnetism in freestanding electronically phase separated manganite thin filmsLifen Xiang,^{1,*} Peng Cai^{2,3,*}, Qiang Li¹, Qian Shi¹, Tian Miao,¹ Yu Bai,¹ Yang Yu,¹ Fanli Lan,¹ Shuaifei Guo,¹ Guorui Chen¹, Wenbin Wang,^{1,6} Lifeng Yin^{1,4,5,6,‡}, Yuanbo Zhang,^{1,4,5,6} and Jian Shen^{1,4,5,6,7,§}¹State Key Laboratory of Surface Physics, Institute for Nanoelectronic Devices and Quantum Computing, and Department of Physics, Fudan University, Shanghai 200433, China²Department of Physics and Beijing Key Laboratory of Opto-electronic Functional Materials and Micro-nano Devices, Renmin University of China, Beijing 100872, China³Key Laboratory of Quantum State Construction and Manipulation (Ministry of Education), Renmin University of China, Beijing 100872, China⁴Shanghai Research Center for Quantum Sciences, Shanghai 201315, China⁵Collaborative Innovation Center of Advanced Microstructures, Nanjing 210093, China⁶Zhangjiang Fudan International Innovation Center, Fudan University, Shanghai 201210, China⁷Shanghai Branch, CAS Center for Excellence and Synergetic Innovation Center in Quantum Information and Quantum Physics, Shanghai 201315, China (Received 13 October 2023; accepted 26 April 2024; published 30 May 2024)

The physical properties of manganites depend sensitively on their lattice degree of freedom. While lattice parameter can be controlled by growing epitaxial thin films on substrates with different lattice constants or application of high pressure, the range of lattice variation is limited to 2–3% before dislocations start to emerge. In contrast, fabrication of freestanding thin films allows one to change the uniaxial lattice parameter up to 8.2%, which opens up a new platform to investigate emergent phenomena under large lattice-constant change. In this work, we fabricate freestanding $(\text{La}_{2/3}\text{Pr}_{1/3})_{5/8}\text{Ca}_{3/8}\text{MnO}_3$ (LPCMO) thin films and investigate how the physical properties are affected by the absence of substrate. We find large length-scale electronic phase separation is greatly suppressed in the freestanding film after being released from the tensile strain of the SrTiO_3 substrate. Consequently, the ferromagnetism is boosted in the freestanding film. The physical properties of the freestanding LPCMO thin film are observed to be comparable to those of LPCMO thin film epitaxially grown on nearly strain-free substrate, revealing that freestanding thin film retains the intrinsic physical properties of LPCMO system, which provides a reliable platform to study effects of large strain and strain gradient (by curvature) in manganite systems.

DOI: [10.1103/PhysRevMaterials.8.054417](https://doi.org/10.1103/PhysRevMaterials.8.054417)**I. INTRODUCTION**

Electronic phases intertwining in quantum materials with strong electronic correlation is not only intriguing from a scientific point of view, but also promising in exploring novel functional materials and electronic devices, which have been widely studied in high-temperature superconductors, heavy fermions, and colossal magnetoresistance (CMR) materials [1]. Strain and pressure are often utilized to manipulate these quantum materials in which the electrons and their interactions are closely coupled to the lattice. To clarify the evolution of intertwined phases upon changing of lattice, investigation of the same piece of sample (even on the same area (atoms) [2]) offers the most ideal methodology. However, tunability of lattice degree of freedom in correlated oxide materials is

limited on single-sample platform, especially compatible with characterization tools for various physical properties.

Take CMR perovskite manganites for example; multiple phases are tightly coupled to lattice in this strongly correlated electron system. At different carrier concentration, various magnetic and electronic ground states can be stabilized in corresponding bond network configuration formed by the MnO_6 octahedra with structural Jahn-Teller distortions. The structure modification is believed to result in mediating the magnetic-exchange interaction between $3d$ electrons on the neighboring sites, while the magnetic field turns the insulating phases into ferromagnetic metallic (FMM) state, resulting in the CMR phenomena. Among the CMR manganites, $(\text{La}_{1-y}\text{Pr}_y)_{1-x}\text{Ca}_x\text{MnO}_3$ (LPCMO) stands as a prototypical system for the strikingly large length-scale electronic phase separation (EPS) between FMM and antiferromagnetic (AFM) charge-ordered insulating (COI) phases, as schematically shown in Fig. 1(a). The lattice strain [3] and quenched disorder [4] have been proposed theoretically to understand such a large-scale electronic phase separation (EPS) in the presence of short-range exchange interaction and long-range Coulomb repulsion force. The recent experiments have shown

*These authors contributed equally to this work.

†pcai@ruc.edu.cn

‡lifengyin@fudan.edu.cn

§shenj5494@fudan.edu.cn

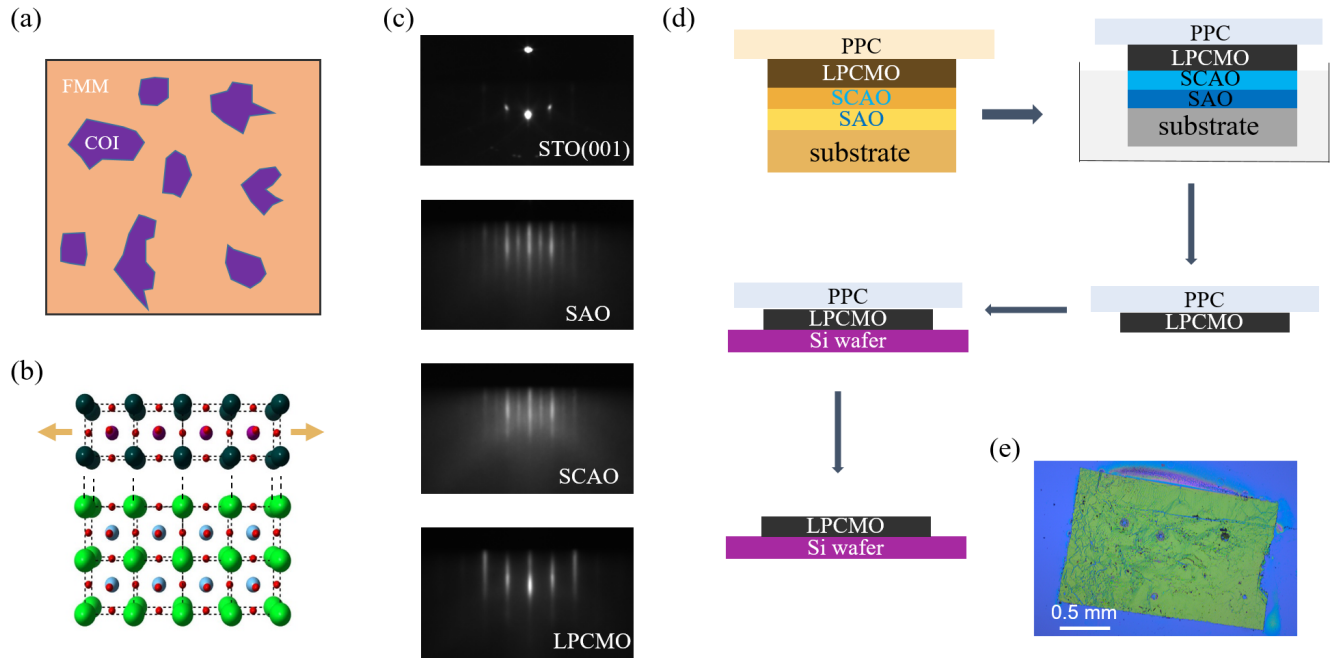


FIG. 1. Fabrication of the freestanding LPCMO film. (a) The electronic phase separation state in LPCMO system with COI domains embedded in FMM domains. (b) Schematic illustrating the epitaxial films grown on substrates. The epitaxial films are strained by the substrates. (c) The RHEED patterns of the STO substrate and SAO, SCAO, and LPCMO films. (d) The schematical release procedure of the freestanding LPCMO film onto the Si wafer. After the sacrificial layers SAO and SCAO being dissolved by deionized water, the LPCMO film was separated with STO substrate and supported by PPC. Then, the LPCMO/PPC can be attached to Si wafer. By dissolving the PPC via acetone, LPCMO film is successfully transferred to Si wafer. (e) Optical microscope image of the freestanding LPCMO film transferred to Si wafer.

that the fully chemically ordered $\text{LaMnO}_3/\text{CaMnO}_3/\text{PrMnO}_3$ superlattice has an AFM insulating ground state without EPS [5]. However, FMM EPS nanonetwork forms again as a consequence of an internal strain relaxation triggered by the structural domain formation of the underlying SrTiO_3 (STO) substrate at low temperatures [6], which implies that both the lattice strain and quenched disorder are important.

Application of pressure is ideal to compress the lattice on the same sample; however, it remains challenging to access the magnetic properties and microscopic structure at nanoscale resolution during experiments [7,8]. By lattice mismatch between a thin film and its underlying substrate as shown in Fig. 1(b), the LPCMO thin film can be modulated by epitaxial strain [9–13]. Thin film on substrates is ideal for the physical property characterization and accessible for nanoscale imaging experiments [14,15]; however, strain-dependent experiments are not accessible to perform on the same thin film since they are grown on the different substrates with discrete lattice parameter. The strain of thin film can also be tuned by piezoelectric substrate which is compatible with real-space experiment [16–19]; however, the polarization of substrate may also change interface and bulk state of manganite by proximity effect [20]. Recently, by developing freestanding oxide membrane [21–24], the FMM state can be successfully tuned into insulating state on the same freestanding $\text{La}_{0.7}\text{Ca}_{0.3}\text{MnO}_3$ membrane by applying tensile strain. It is believed that freestanding LPCMO membrane with EPS would bring an ideal platform to investigate how elastic strain fields affect the correlated states; however, it is unknown if such freestanding LPCMO membrane has been achieved yet.

In this work, we focus on $(\text{La}_{2/3}\text{Pr}_{1/3})_{5/8}\text{Ca}_{3/8}\text{MnO}_3$, and find the large-scale EPS is suppressed in freestanding LPCMO film, as the tensile strain is released from the as-grown sample, unambiguously clarifying that the EPS can be tuned by lattice strain in LPCMO system. Moreover, by carrying out experiments with spatial resolution, we also demonstrate that freestanding LPCMO film may provide a platform to study the EPS phenomena upon strain engineering.

II. EXPERIMENTS

To prepare a freestanding LPCMO membrane, multilayer heterostructure consisting of sacrificial buffer layers and 76.8-nm-thick LPCMO on the single-crystalline STO (001) substrate by using pulsed laser deposition (PLD). The lattice of LPCMO is around 3.84 Å, much smaller than that of the water-soluble buffer layer $\text{Sr}_3\text{Al}_2\text{O}_6$ (SAO). To reduce the giant lattice mismatch between SAO and the LPCMO films [22,25], another water-soluble $\text{SrCa}_2\text{Al}_2\text{O}_6$ (SCAO, Ca-substituted SAO) thin layer with reduced lattice constant is inserted between SAO and LPCMO layer. Reflection high-energy electron diffraction (RHEED) was used to monitor the layer-by-layer growth, and the RHEED patterns of each type of layer are in Fig. 1(c). Figure 1(d) shows the schematical release procedure of the freestanding LPCMO film onto the Si wafer. The polypropylene carbonate (PPC) was used to support the LPCMO film during the release process. As the PPC/LPCMO/SCAO/SAO/STO stack was immersed in deionized water at room temperature, SAO and SCAO buffer layers were selectively etched so that LPCMO

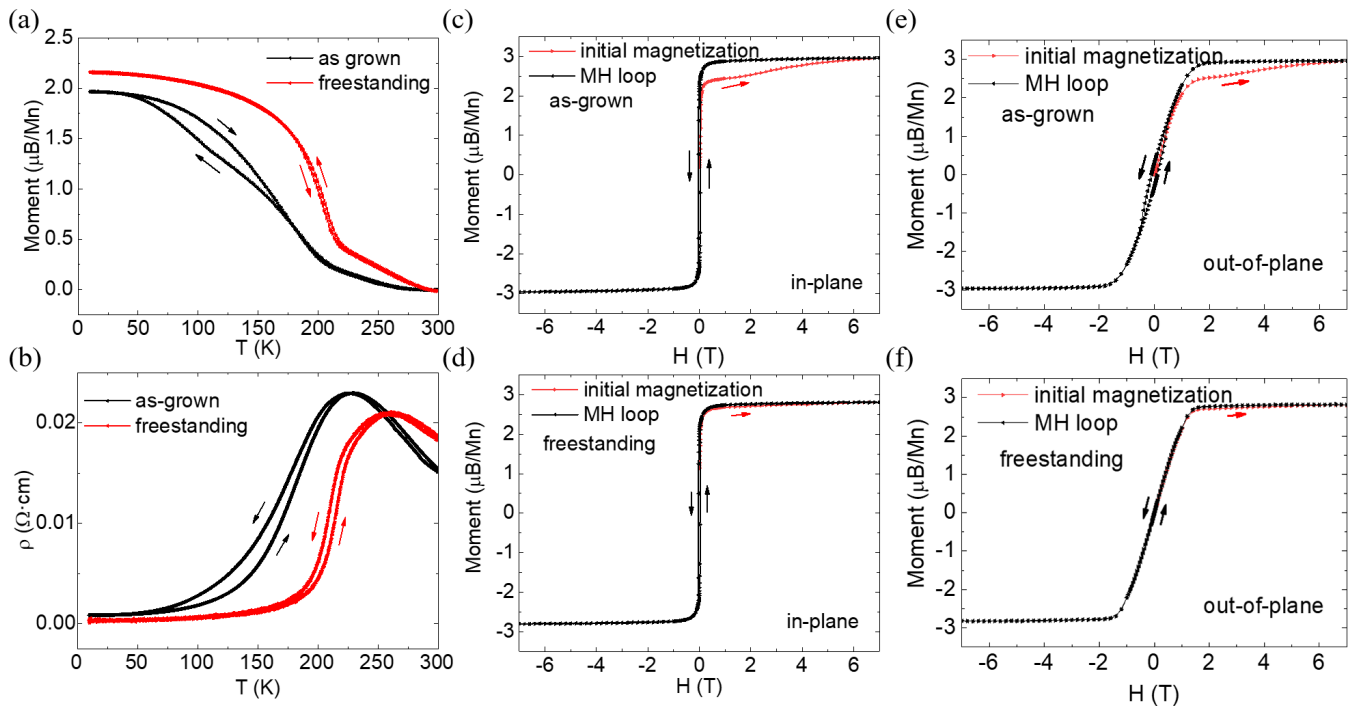


FIG. 2. Comparison between the as-grown and freestanding LPCMO films. Temperature-dependent (a) magnetization and (b) resistivity curves of the as-grown LPCMO film (black dotted lines), before being released from STO substrate, and the freestanding LPCMO film (red dotted lines). The cooling and warming magnetizations are measured in 200 Oe with in-plane magnetic field. The resistivity is measured at zero magnetic field. The in-plane magnetic field-dependent magnetization curves of the (c) as-grown and (d) freestanding LPCMO films. The out-of-plane magnetic field-dependent magnetization curves of (e) the as-grown and (f) freestanding LPCMO films. The red dotted lines represent the initial magnetization curves.

film was separated from STO substrate and then left on the PPC. Then, PPC/LPCMO was stamped on Si wafer. After dissolving the PPC, the freestanding LPCMO film was transferred and released onto Si wafer. Figure 1(e) presents the typical freestanding LPCMO sample transferred onto Si wafer. The electrodes were deposited on the freestanding LPCMO sample to characterize the electric properties. To get intrinsic magnetic properties, the magnetic characterizations of LPCMO film were done before electrode deposition.

III. RESULTS AND DISCUSSION

Figures 2(a) and 2(b) show the temperature dependence of magnetization ($M-T$) and resistivity ($R-T$) curves of the freestanding film. For comparison, the behavior of the same LPCMO film grown on substrate before release (dubbed “as-grown” LPCMO thin film) was also investigated. The most unique feature in as-grown LPCMO thin film is the dramatic thermal hysteresis in both $R-T$ and $M-T$ curves, remarking the famous large-scale EPS of FMM and COI states’ transition from paramagnetic insulating state [14,26]. As shown in the $M-T$ curve, the FMM phase grows with decreasing temperature and forms the long-range ferromagnetic order at 174 K ($T_c \sim 174$ K, determined by the derivative of $M-T$ curve). The percolation of the FMM phase also leads to the insulator-to-metal transition around T_c in the $R-T$ curve. Some FMM states are transitioned from COI states upon cooling to base temperature, while they are not reversely transitioned into

COI upon warming from base temperature at same temperature, resulting in the dramatic hysteresis of $M-T$ and $R-T$. After release from the substrate, this dramatic hysteresis almost disappeared in the freestanding LPCMO sample, indicating a strong suppression of large-scale EPS. Moreover, the T_c of long-range ferromagnetic order and the metal-insulating transition temperature (T_{MIT}) are both significantly increased in freestanding LPCMO film, revealing the enhancement of FMM state. As to the freestanding film, T_{co} and T_c are 260 and 203 K, respectively, determined by the derivation of $M-T$ curve (Fig. S3 in Supplemental Material [27]). The magnetic moments of FM clusters ($T_c < T < T_{co}$) [28] and uncompensated spin at the edges of CO clusters ($T > T_{co}$) [15,29–31] give the small magnetic signal above T_c and T_{co} in Fig. 2(a), respectively. To get further detailed information about the magnetic and electronic state of freestanding LPCMO film, field dependence of magnetization in freestanding and as-grown LPCMO film is investigated at base temperature after zero-field cooling. Figure 2(c) shows the magnetic anisotropy of the as-grown LPCMO films with both in-plane and out-of-plane magnetic hysteresis measured by a superconducting quantum interference device (SQUID). The hysteresis loops show that the easy magnetization axis of the thin films lies in the film plane which is attributed to the shape anisotropy of the thin films. The peculiar initial magnetization curve of the as-grown LPCMO film [red curve in Fig. 2(c)] shows that upon application of magnetic field, the COI phase melted into FMM phase, indicating the coexistence of COI and FMM states even

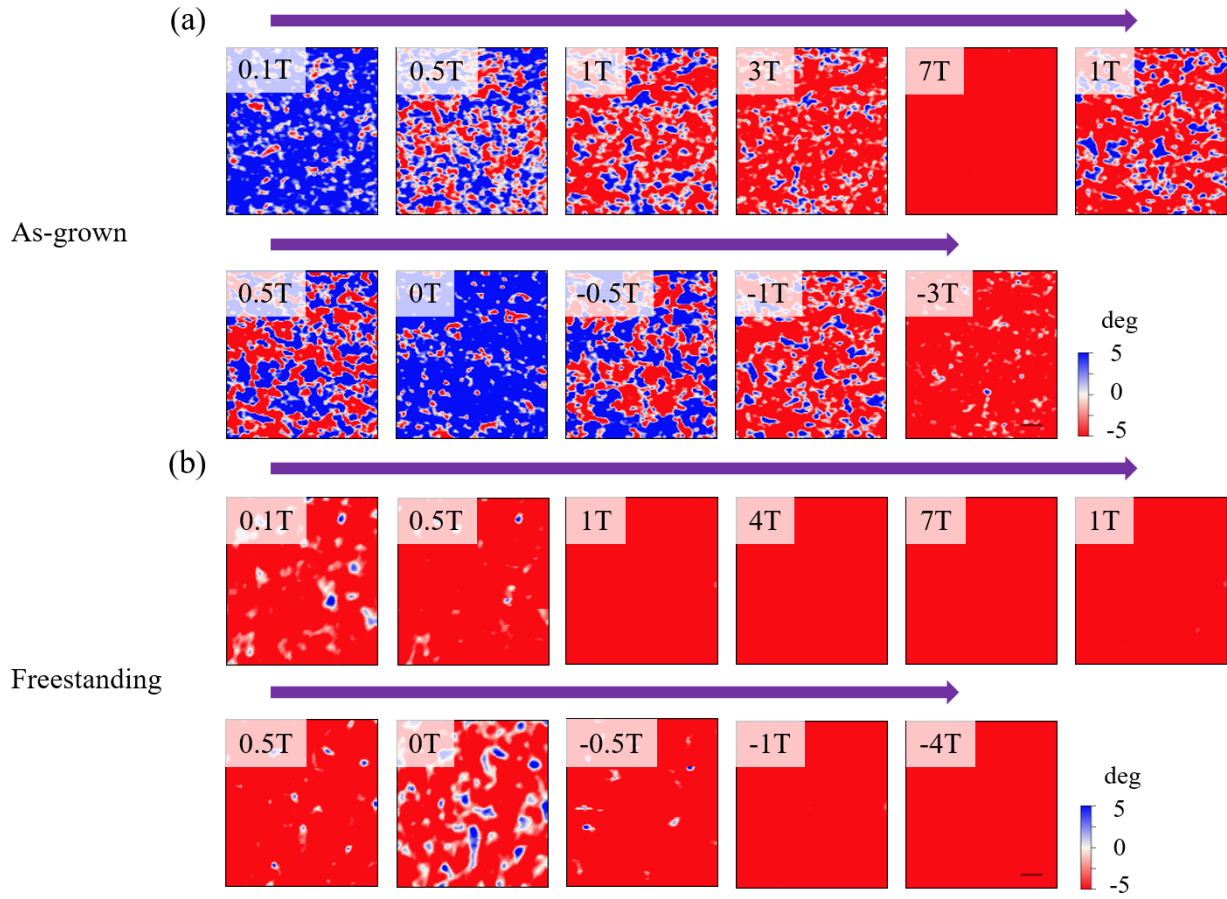


FIG. 3. The MFM phase images of the (a) as-grown, and (b) freestanding LPCMO films. The MFM images were acquired after the system was zero-field cooled down to around 10 K. The scale bar here is 1 μm . When magnetic field increased from 0.1 to 7 T, the FMM phase domains (negative signal) merged, and the COI phase domains (positive signal) gradually melt into FMM phase.

at 10 K [14,26,32]. The postinitial magnetization curve has no hysteresis representing a typical behavior for a ferromagnetic system, different from the initial magnetization curve, since the EPS almost disappears as COI state melts into FMM state. After release, the initial magnetization curve shows no sign of COI melting for the freestanding LPCMO film as shown in Fig. 2(d), revealing nearly the absence of COI state and thus strong suppression of EPS. In addition, the FMM phase volume fraction can also be estimated in the initial magnetization curves [33,34]. The FMM volume fraction of the as-grown LPCMO film is smaller than that of the freestanding LPCMO film. Overall, the hysteresis of M - T and R - T curves and the characteristic initial magnetization curves feature the EPS in manganites [26,35]. By comparison with as-grown LPCMO film, the behavior of freestanding sample (we remind that the comparison is done on the same sample) reveals that the COI states are suppressed after the sample is released, indicative of enhancement of FMM states and suppression of EPS as well.

To further uncover the microscopic magnetic structure of the as-grown and freestanding LPCMO films, magnetic force microscope (MFM) [14] is used to map out the real-space magnetic domain distribution at base temperature (10 K) after zero-field cooling. For MFM imaging, soft (coercivity

~ 100 Oe) magnetic tips have been used. The detailed principle of the MFM measurements is explained in the Supplemental Material [27]. When an out-of-plane magnetic field is applied, the magnetization of the FMM regions will have a component in the out-of-plane direction, which applies an attraction force to the MFM tip leading to a negative shift in phase. Due to the closed loop of the magnetic flux, the COI regions will generate a zero or positive phase shift [14,15]. Figure 3(a) shows the magnetic-field dependent MFM images of the as-grown LPCMO film, capturing the evolution of magnetic state with large-scale EPS. Various FMM domains are visualized at nearly zero field. As the magnetic field is applied along hard axis (out-of-plane direction), more and more FMM domains (red patch) line up in the initial magnetization procedure (0.1 – 7 T) and fully polarize at 7 T. The almost identical MFM pattern at 1 and -1 T in postinitial magnetization shows more FMM than that observed in 1 T in the initial magnetization, indicating there are COI states melted into stable FMM state in the magnetization [14]. In contrast to as-grown LPCMO, the FMM domain in the freestanding LPCMO film as shown in Fig. 3(b) is dominant, illustrating the enhancement of ferromagnetic order. Nearly no blue patches are observed at 1 T, indicating the absence of COI state. These results are consistent with the macroscopic

TABLE I. The in-plane and out-of-plane lattice constant and the Curie temperature (T_c) of the as-grown, freestanding, and strain-free LPCMO films.

LPCMO film	Lattice constant in plane (nm)	Lattice constant out of plane (nm)	Curie temperature T_c (K)
As-grown	0.386	0.382	174
Freestanding	0.384	0.385	203
Strain-free	0.385	0.384	206

magnetization measurements, illustrating the suppression of COI phase and the enhancement of FMM phase in the freestanding LPCMO film.

The lattice constant is determined to understand the origin of the suppression of EPS in freestanding LPCMO film, as the freestanding sample is released from the as-grown one. Table I summarizes the in-plane and out-of-plane lattice constants obtained from x-ray reciprocal-space maps (RSM). The in-plane lattice constant of as-grown LPCMO film is around 3.86 Å, because of tensile strain from the sacrificial layers with in-plane lattice constant slightly larger than that of bulk LPCMO. After release, the in-plane lattice constant shrinks while out-of-plane lattice constant increases, manifesting the strain is released when the epitaxial LPCMO film is separated with substrate and the freestanding LPCMO film has tendency to return to a bulklike structure, consistent with the similar experiments [36,37]. The enhancement of FMM phase and suppression of EPS in freestanding LPCMO can be attributed to *in situ* strain release.

To further examine the strain effect on EPS, we have also grown 76.8-nm-thick LPCMO film with identical parameters on SrLaGaO₄ (001) (SLGO) substrate (dubbed “strain-free” LPCMO film), since the LPCMO film is believed to be nearly unstrained due to the excellent lattice match between LPCMO and SLGO substrate [9]. The SLGO substrate is single-phase tetragonal structure with space group $I4/mmm$. In addition to having similar lattice constant and T_c (Table I), freestanding film and the nearly strain-free LPCMO film exhibit very similar properties, as shown in Figs. 4(a)–4(d). No obvious hysteresis in M - T or R - T curves can be seen in both films. Moreover, their initial magnetization curves are both almost inside the M - H loops, indicating similar suppression of large-scale EPS in both films. Note that the difference of the resistivity between these two samples can be attributed to the transfer process, which may introduce some local defects leading to a higher resistivity in the freestanding film. The near-identical behavior between the freestanding thin film and the film grown on lattice-matched substrate ensures the fact that freestanding thin film retains the intrinsic physical properties of the LPCMO system.

To unveil the strain effect on CMR, the temperature dependence of magnetoresistance (MR) with field cooling is carefully investigated in as-grown, freestanding, and strain-free LPCMO films, as revealed in Fig. 4(e). The magnetic field is 9 T, which is strong enough to melt the COI phase into FMM phase in field-cooling process. The temperature dependence of MR shows a peak near T_c for all these three films, illustrating CMR in LPCMO is also affected by strain in accordance with the shift of T_c . The discrepancy in MR values between the strain-free and freestanding LPCMO films

may be caused by different EPS percolation process, which is closely tied to the distribution characteristics of EPS domains (scale, density, shape, etc.) as well as the dynamics of percolation of EPS (nucleation, growth, domain-wall pinning, etc.). Due to the release process of the freestanding film, some defects may be introduced which may ultimately affect these EPS characteristics and thus CMR values.

The enhancement of ferromagnetism and suppression of large-scale EPS in freestanding film can be naturally ascribed to strain effect, since the only differences between the as-grown and freestanding LPCMO films are the lattice parameter, such as the change of the Mn–O bond length and Mn–O–Mn bond angle. On the one hand, the shrink of the lattice constant makes the hopping increase between the e_g orbitals of Mn ions and the p orbitals of oxygen ions, leading to enhanced double-exchange interaction and hence favoring FMM phase [38,39], consistent with previous experiment controlled by hydrostatic pressure and compressive strain [40–43]. On the other hand, the lowered symmetry by the tensile strain [Fig. 4(f)] can induce Jahn-Teller distortion to stabilize COI phases [7,22,44–49], leading to competition and coexistence of COI and FMM states in as-grown LPCMO film. Overall, by the *in situ* strain-release process, the lattice effect is found to be crucial to manipulate the EPS in manganese. For freestanding and strain-free LPCMO films with nearly the same lattice constant of bulk form, even though these two samples are not the same, they share similar thermal hysteresis of magnetic and electric properties and comparable T_c . The overall similarity of electric and magnetic properties hints that the lattice effect plays a major role in manipulating these magnetic orders and EPS.

IV. CONCLUSION

As a summary, using water-soluble sacrificial buffer layers, the freestanding LPCMO film can be obtained, accompanied by strain release to that of the bulk form. The electric and magnetic properties of freestanding LPCMO film are carefully characterized, unambiguously demonstrating that the EPS is tunable by lattice strain. As the strain is released, the FMM state is enhanced while EPS is suppressed in freestanding thin film. It also provides a promising platform for systematic study of EPS on the same area upon application of reversible (continuously) tunable strain, which had been successfully performed in previous works [22,25]. Note that as the geometry is reduced to two-dimensional (2D) limit, many quantum materials exhibit properties different from that in its bulk form [50–53]. Moreover, many unexpected states emerge in freestanding 2D materials released from its substrate, such as BaFeO₃ with large polarization [23], STO with

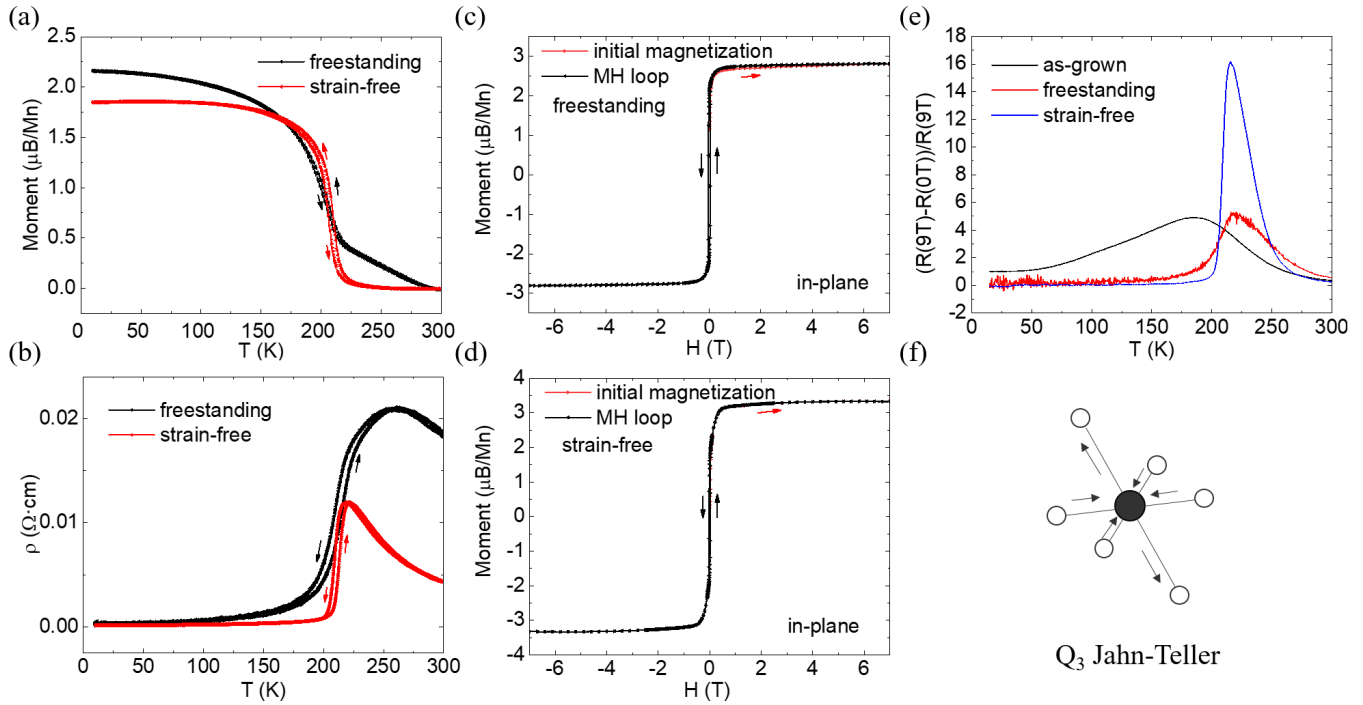


FIG. 4. Comparison between the freestanding and strain-free LPCMO films under the strain. Temperature-dependent (a) magnetization and (b) resistivity curves of the freestanding LPCMO film (black dotted lines) and the strain-free LPCMO film grown on SLGO (001) (red dotted lines). The cooling and warming magnetization curves are measured in 200 Oe with in-plane magnetic field. The resistivity is measured at zero magnetic field. The in-plane magnetic field-dependent magnetization curves of the (c) freestanding and (d) strain-free LPCMO films. The initial magnetization curves (red lines) of the freestanding and strain-free LPCMO films are almost inside the hysteresis loops (black lines). (e) The temperature-dependent magnetoresistance under 9 T of the as-grown (black line), freestanding (red line), and strain-free (blue line) LPCMO films. (f) The Q_3 -mode Jahn-Teller distortion.

room-temperature ferroelectricity [25], and $\text{La}_{0.7}\text{Ca}_{0.3}\text{MnO}_3$ with exotic order of spin and charge [22]. Freestanding LPCMO ultrathin film would also provide a novel routine to explore and manipulate the EPS phenomena down to 2D limit.

V. METHODS

A. Epitaxial film fabrication

The $\text{Sr}_3\text{Al}_2\text{O}_6$ and $\text{SrCa}_2\text{Al}_2\text{O}_6$ layers were successively grown on TiO_2 -terminated SrTiO_3 (001) substrate by PLD (248-nm KrF excimer laser, 2-Jcm^{-2} fluence, 5 Hz) at 850°C . The oxygen pressure was 5×10^{-6} mbar, containing 10% ozone. Then $(\text{La}_{2/3}\text{Pr}_{1/3})_{5/8}\text{Ca}_{3/8}\text{MnO}_3$ (LPCMO) film was grown on the top of buffer layers using 1.5-Jcm^{-2} laser fluence, 5 Hz at the substrate temperature of 830°C , and the oxygen pressure was 9×10^{-4} mbar containing 10% ozone. During the growth, the RHEED was used to monitor the layer-by-layer growth mode. With the same LPCMO film growth parameter, the LPCMO was grown on single-crystal SrLaGaO_4 (001) substrate to obtain the strain-free LPCMO film.

B. Release of the freestanding films

The polypropylene carbonate first was adhered to the surface of the as-grown LPCMO film by spin coating. Then, the whole structure was immersed into deionized water at room

temperature to dissolve the sacrificial buffer layers [Fig. 1(c)]. After water etching, the freestanding film on PPC was attached to the Si wafer. The freestanding film remained on Si wafer after dissolving the PPC by acetone.

C. Measurements

Magnetization measurements were conducted on a Quantum Design SQUID. Transport measurements were conducted in a four-point geometry on a physical property measurement system. MFM measurements were carried out in the attoDRY 1000-9T system with scanning probe microscope (Attocube). Commercial Co/Cr-coated tips were used. The dual-pass mode was put into use to reduce the topographic contribution. In the first scan, the topography of the sample was obtained in tapping mode. Then, the tip would be lifted around 90 nm to the sample surface and scanned following the line profile of the first scan to acquire magnetic signal from the sample. The x-ray-diffraction data were carried out in the Bruker D8 A25 Discover. The out-of-plane lattice constants of the as-grown, freestanding, and strain-free LPCMO films were calculated by the Bragg equation and the diffraction angle was obtained from the 2θ - ω scan. The in-plane lattice constant was estimated from the RSM of the LPCMO films. The (103) peak of the LPCMO films contains the in-plane and out-of-plane lattice constant.

ACKNOWLEDGMENTS

This work was supported by National Key Research Program of China (Grants No. 2022YFA1403300 and No. 2022YFA1403102), National Natural Science Foundation of China (Grants No. 111427902, No. 11991060, No. 12074075, No. 12074071, and No. 12074424), Shanghai Municipal Sci-

ence and Technology Major Project No. 2019SHZDZX01, Shanghai Municipal Natural Science Foundation (Grants No. 20501130600 and No. 22ZR1407400), Open Research Fund Program of the State Key Laboratory of Low-Dimensional Quantum Physics, the Fundamental Research Funds for the Central Universities, and the Research Funds of Renmin University of China.

- [1] E. Dagotto, *Science* **309**, 257 (2005).
- [2] P. Cai, X. D. Zhou, W. Ruan, A. F. Wang, X. H. Chen, D. H. Lee, and Y. Y. Wang, *Nat. Commun.* **4**, 1596 (2013).
- [3] K. H. Ahn, T. Lookman, and A. R. Bishop, *Nature (London)* **428**, 401 (2004).
- [4] J. Burgy, M. Mayr, V. Martin-Mayor, A. Moreo, and E. Dagotto, *Phys. Rev. Lett.* **87**, 277202 (2001).
- [5] T. Miao, L. N. Deng, W. T. Yang, J. Y. Ni, C. L. Zheng, J. Etheridge, S. S. Wang, H. Liu, H. X. Lin, Y. Yu, Q. Shi, P. Cai, Y. Y. Zhu, T. Y. Yang, X. M. Zhang, X. Y. Gao, C. Y. Xi, M. L. Tian, X. S. Wu, H. J. Xiang, E. Dagotto, L. F. Yin, and J. Shen, *Proc. Natl. Acad. Sci. USA* **117**, 7090 (2020).
- [6] Q. Li, T. Miao, H. M. Zhang, W. Y. Lin, W. H. He, Y. Zhong, L. F. Xiang, L. N. Deng, B. Y. Ye, Q. Shi, Y. Y. Zhu, H. W. Guo, W. B. Wang, C. L. Zheng, L. F. Yin, X. D. Zhou, H. J. Xiang, and J. Shen, *Nat. Commun.* **13**, 6593 (2022).
- [7] Z. X. Zhang, J. F. Shao, F. Jin, K. J. Dai, J. Y. Li, D. Lan, E. D. Hua, Y. Y. Han, L. Wei, F. Cheng, B. H. Ge, L. F. Wang, Y. Zhao, and W. B. Wu, *Nano Lett.* **22**, 7328 (2022).
- [8] A. Jayaraman, *Rev. Mod. Phys.* **55**, 65 (1983).
- [9] D. Gillaspie, J. X. Ma, H. Y. Zhai, T. Z. Ward, H. M. Christen, E. W. Plummer, and J. Shen, *J. Appl. Phys.* **99**, 08S901 (2006).
- [10] J. Dho, Y. N. Kim, Y. S. Hwang, J. C. Kim, and N. H. Hur, *Appl. Phys. Lett.* **82**, 1434 (2003).
- [11] T. Wu, S. B. Ogale, S. R. Shinde, A. Biswas, T. Polletto, R. L. Greene, T. Venkatesan, and A. J. Millis, *J. Appl. Phys.* **93**, 5507 (2003).
- [12] Y. Y. Zhao, J. Wang, F. X. Hu, H. Kuang, Y. Liu, J. R. Sun, and B. G. Shen, *IEEE Trans. Magn.* **51**, 4400804 (2015).
- [13] W. G. Wei, H. Wang, K. Zhang, H. Liu, Y. F. Kou, J. J. Chen, K. Du, Y. Y. Zhu, D. L. Hou, R. Q. Wu, L. F. Yin, and J. Shen, *Chin. Phys. Lett.* **32**, 087504 (2015).
- [14] H. Liu, L. F. Lin, Y. Yu, H. X. Lin, Y. Y. Zhu, T. Miao, Y. Bai, Q. Shi, P. Cai, Y. F. Kou, F. L. Lan, W. B. Wang, X. D. Zhou, S. Dong, L. F. Yin, and J. Shen, *Phys. Rev. B* **96**, 195154 (2017).
- [15] K. Du, K. Zhang, S. Dong, W. G. Wei, J. Shao, J. B. Niu, J. J. Chen, Y. Y. Zhu, H. X. Lin, X. L. Yin, S. H. Liou, L. F. Yin, and J. Shen, *Nat. Commun.* **6**, 6179 (2015).
- [16] M. C. Dekker, A. D. Rata, K. Boldyreva, S. Oswald, L. Schultz, and K. Dorr, *Phys. Rev. B* **80**, 144402 (2009).
- [17] J. F. Wang, Y. C. Jiang, Z. P. Wu, and J. Gao, *Appl. Phys. Lett.* **102**, 071913 (2013).
- [18] M. Zheng, X. Y. Li, M. M. Yang, Q. X. Zhu, Y. Wang, X. M. Li, X. Shi, H. L. W. Chan, X. G. Li, H. S. Luo, and R. K. Zheng, *Appl. Phys. Lett.* **103**, 263507 (2013).
- [19] T. Zhang, Q. Wei, R. K. Zheng, X. P. Wang, and Q. F. Fang, *J. Appl. Phys.* **113**, 013705 (2013).
- [20] A. Frano, S. Blanco-Canosa, E. Schierle, Y. Lu, M. Wu, M. Bluschke, M. Minola, G. Christiani, H. U. Habermeier, G. Logvenov, Y. Wang, P. A. van Aken, E. Benckiser, E. Weschke, M. Le Tacon, and B. Keimer, *Nat. Mater.* **15**, 831 (2016).
- [21] D. Lu, D. J. Baek, S. S. Hong, L. F. Kourkoutis, Y. Hikita, and H. Y. Hwang, *Nat. Mater.* **15**, 1255 (2016).
- [22] S. S. Hong, M. Q. Gu, M. Verma, V. Harbola, B. Y. Wang, D. Lu, A. Vailionis, Y. Hikita, R. Pentcheva, J. M. Rondinelli, and H. Y. Hwang, *Science* **368**, 71 (2020).
- [23] D. X. Ji, S. H. Cai, T. R. Paudel, H. Y. Sun, C. C. Zhang, L. Han, Y. F. Wei, Y. P. Zang, M. Gu, Y. Zhang, W. P. Gao, H. X. Huyan, W. Guo, D. Wu, Z. B. Gu, E. Y. Tsympal, P. Wang, Y. F. Nie, and X. Q. Pan, *Nature (London)* **570**, 87 (2019).
- [24] G. H. Dong, S. Z. Li, M. T. Yao, Z. Y. Zhou, Y. Q. Zhang, X. Han, Z. L. Luo, J. X. Yao, B. Peng, Z. Q. Hu, H. B. Huang, T. T. Jia, J. Y. Li, W. Ren, Z. G. Ye, X. D. Ding, J. Sun, C. W. Nan, L. Q. Chen, J. Li, and M. Liu, *Science* **366**, 475 (2019).
- [25] R. J. Xu, J. W. Huang, E. S. Barnard, S. S. Hong, P. Singh, E. K. Wong, T. Jansen, V. Harbola, J. Xiao, B. Y. Wang, S. Crossley, D. Lu, S. Liu, and H. Y. Hwang, *Nat. Commun.* **11**, 3141 (2020).
- [26] M. Uehara, S. Mori, C. H. Chen, and S. W. Cheong, *Nature (London)* **399**, 560 (1999).
- [27] See Supplemental Material at <http://link.aps.org/supplemental/10.1103/PhysRevMaterials.8.054417> for the interpretation of the MFM measurement; the measurements of x-ray rocking curves of three LPCMO films; the determination of Curie temperature and the charge-order temperature of the freestanding LPCMO film. The Supplemental Material also contains Refs. [14, 15].
- [28] A. Moreo, S. Yunoki, and E. Dagotto, *Science* **283**, 2034 (1999).
- [29] B. Hermsmeier, J. Osterwalder, D. J. Friedman, and C. S. Fadley, *Phys. Rev. Lett.* **62**, 478 (1989).
- [30] J. Hemberger, A. Krimmel, T. Kurz, H.-A. K. Krug von Nidda, V. Yu. Ivanov, A. A. Mukhin, A. M. Balbashov, and A. Loidl, *Phys. Rev. B* **66**, 094410 (2002).
- [31] L. L. Chen, J. Y. Fan, W. Tong, D. Z. Hu, L. Zhang, L. S. Ling, L. Pi, Y. H. Zhang, and H. Yang, *J. Mater. Sci.* **53**, 323 (2018).
- [32] L. F. Xiang, Y. Shi, W. Chao, H. Y. Zhang, Q. Li, W. J. Hu, W. B. Wang, H. W. Guo, C. L. Zheng, J. Etheridge, L. F. Yin, Y. Y. Zhu, X. D. Zhou, and J. Shen, *Appl. Phys. Lett.* **122**, 112402 (2023).
- [33] Y. Y. Zhu, K. Du, J. B. Niu, L. F. Lin, W. G. Wei, H. Liu, H. X. Lin, K. Zhang, T. Y. Yang, Y. F. Kou, J. Shao, X. Y. Gao, X. S. Xu, X. S. Wu, S. Dong, L. F. Yin, and J. Shen, *Nat. Commun.* **7**, 11260 (2016).
- [34] J. X. Ma, D. T. Gillaspie, E. W. Plummer, and J. Shen, *Phys. Rev. Lett.* **95**, 237210 (2005).
- [35] J. Shao, H. Liu, K. Zhang, Y. Yu, W. C. Yu, H. X. Lin, J. B. Niu, K. Du, Y. F. Kou, W. G. Wei, F. L. Lan, Y. Y. Zhu, W. B.

- Wang, J. Xiao, L. F. Yin, E. W. Plummer, and J. Shen, *Proc. Natl. Acad. Sci. USA* **113**, 9228 (2016).
- [36] Z. Y. Chen, B. Y. Wang, B. H. Goodge, D. Lu, S. S. Hong, D. F. Li, L. F. Kourkoutis, Y. Hikita, and H. Y. Hwang, *Phys. Rev. Mater.* **3**, 060801(R) (2019).
- [37] P. T. P. Le, J. E. ten Elshof, and G. Koster, *Sci. Rep.* **11**, 12435 (2021).
- [38] A. J. Millis, T. Darling, and A. Migliori, *J. Appl. Phys.* **83**, 1588 (1998).
- [39] Y. Moritomo, A. Asamitsu, and Y. Tokura, *Phys. Rev. B* **51**, 16491 (1995).
- [40] J. J. Neumeier, M. F. Hundley, J. D. Thompson, and R. H. Heffner, *Phys. Rev. B* **52**, R7006 (1995).
- [41] Y. Moritomo, H. Kuwahara, Y. Tomioka, and Y. Tokura, *Phys. Rev. B* **55**, 7549 (1997).
- [42] I. Medvedeva, A. Maignan, K. Barner, Y. Bersenev, A. Roev, and B. Raveau, *Physica B* **325**, 57 (2003).
- [43] H. K. Jani, D. V. M. Repaka, and R. Mahendiran, *J. Appl. Phys.* **113**, 17D721 (2013).
- [44] Z. Fang, I. V. Solovyev, and K. Terakura, *Phys. Rev. Lett.* **84**, 3169 (2000).
- [45] F. Rivadulla, M. A. Lopez-Quintela, J. Mira, and J. Rivas, *Phys. Rev. B* **64**, 052403 (2001).
- [46] Y. Ding, D. Haskel, Y. C. Tseng, E. Kaneshita, M. van Veenendaal, J. F. Mitchell, S. V. Sinogeikin, V. Prakapenka, and H. K. Mao, *Phys. Rev. Lett.* **102**, 237201 (2009).
- [47] F. Jin, Q. Y. Feng, Z. Guo, D. Lan, L. F. Wang, G. Y. Gao, H. R. Xu, B. B. Chen, F. Chen, Q. Y. Lu, and W. B. Wu, *Phys. Rev. Mater.* **1**, 064406 (2017).
- [48] J. Klein, J. B. Philipp, G. Carbone, A. Vigliante, L. Alff, and R. Gross, *Phys. Rev. B* **66**, 052414 (2002).
- [49] T. Hotta, A. Feiguin, and E. Dagotto, *Phys. Rev. Lett.* **86**, 4922 (2001).
- [50] J. Z. Sun, D. W. Abraham, R. A. Rao, and C. B. Eom, *Appl. Phys. Lett.* **74**, 3017 (1999).
- [51] M. Huijben, L. W. Martin, Y. H. Chu, M. B. Holcomb, P. Yu, G. Rijnders, D. H. A. Blank, and R. Ramesh, *Phys. Rev. B* **78**, 094413 (2008).
- [52] A. Tebano, A. Orsini, P. G. Medaglia, D. Di Castro, G. Balestrino, B. Freelon, A. Bostwick, Y. J. Chang, G. Gaines, E. Rotenberg, and N. L. Saini, *Phys. Rev. B* **82**, 214407 (2010).
- [53] H. Y. Chen, Y. Yu, Z. Wang, Y. Bai, H. X. Lin, X. L. Li, H. Liu, T. Miao, Y. F. Kou, Y. S. Zhang, Y. Li, J. Tang, Z. C. Wang, P. Cai, Y. Y. Zhu, Z. H. Cheng, X. Y. Zhong, W. B. Wang, X. Y. Gao, L. F. Yin, R. Q. Wu, and J. Shen, *Phys. Rev. B* **99**, 214419 (2019).